Numerical investigation of near-muzzle blast levels for perforated muzzle brake using high performance computing

Ilya Semenov[1,2], Pavel Utkin[1,2], Ildar Akhmedyanov[1], Igor Menshov[3], Pavel Pasynkov[1,2]

[1]*Institute for Computer Aided Design Russian Academy of Sciences, 19/18 2nd Brestskay str., Moscow, Russia*
[2]*Moscow Institute of Physics and Technology, 9 Institutsky str., Dolgoprudny, Russia*
[3]*Keldysh Institute of Applied Mathematics RAS, 4 Miusskaya sq., Moscow, Russia*

semenov@icad.org.ru, utkin@icad.org.ru

Abstract. *The simultaneous solution of the internal and intermediate ballistics problem is considered by the example of a cannon with muzzle gas dynamics device – perforated muzzle brake. The blast levels are obtained in the near-muzzle field. The investigations are performed by means of numerical experiments using high performance computing on cluster systems. The internal ballistics process study is based on the mathematical model of multiphase multicomponent two-velocity gas-powder continuum motion taking into account powder grains burning and force and energy inter-phase interaction. The projectile motion is described by immersed boundary method when the special source terms are included to the right-hand side of multiphase dynamics equations to model the influence of projectile boundary to the outer flow, and the calculation is performed consistently through the whole computational domain. The description of numerical algorithm parallelization is presented. Results of mathematical modeling are in good agreement with the data from natural experiments.*

Keywords

Internal ballistics, intermediate ballistics, muzzle brake, blast level, immersed boundary method, parallel calculations

1 Introduction

Muzzle brake (MB) is a device in the muzzle part of the cannon barrel which changes the direction of gas powder motion which flows out from the cannon and so reduces the cannon recoil velocity and the gun carriage load [1], [2]. The principle of MB of any construction operation can be summarized by saying that when the powder gases flow out from the side holes the gas mass flow in the axial direction decreases and so the reactive force in the barrel motion direction decreases also. Another MB operating effect is connected with the decrease of the barrel tug due to the shocks which form on the inner parts of the MB when powder gas flows out. Fig. 1 illustrates the outside appearance of several types of muzzle brakes. The side effect of recoil decreasing is the growth of overpressure level in the near-muzzle field. From a designer's perspective, the problem is to choose a cannon-brake system which yields specific values of muzzle velocity and weapon impulse but minimizes the blast increase [3].

(a) chambered (b) slatted (c) perforated

Fig. 1. Different types of muzzle brakes

For the predictive modeling and making recommendations about blast level decreasing for a cannon with MB shot the understanding of the powder gases flow features and their influence on blast wave propagation is necessary. Up to date as a rule the solution of intermediate ballistics problems is carried out apart from the internal ballistics process calculation that demands the agreement of boundary conditions. A good example for that is the investigation [4]. The authors in [4] with the use of three-dimensional gas dynamics calculations determine the force which affects on MB. However it is supposed that at the initial time moment which corresponds to the moment when the projectile enters to the MB the air in the MB is at rest. At the inlet the boundary conditions of specified dependencies of pressure, density velocity and temperature of powder gas against time are set.

The dependencies are obtained from the preliminary internal ballistics calculation which provides the description of the process only up to the time moment when the projectile reaches the muzzle face. Note that in [4] the problem of blast levels determination is not considered. As it is known [5] the complex transient flow structure which forms in outer space before the projectile moves out (see Fig. 5a) have a significant effect on blast levels. The simulation of shock wave which forms before the moving projectile is possible only in case of simultaneous solution of the internal and intermediate ballistics problem.

The goal of the current work is the numerical investigation of blast levels for perforated muzzle brake and comparison of the obtained results with the data of natural experiments [6]. The problem is essentially three-dimensional but the qualitative understanding of muzzle flow features as well as preliminary quantitative parameters can be obtained from the simultaneous solution of the internal and intermediate ballistics problem in axisymmetrical statement.

2 Mathematical model of internal and intermediate ballistics processes

The object of the mathematical model in use is the moving heterogeneous media which is considered as two-phase continuum consisted of dispersed phase of the powder elements and the gaseous phase of powder combustion products. The fundamental principles of the model are explained in the work [7] dedicated to the description of mathematical models, parallel numerical algorithms for the solution of interior ballistics problems in quasi-one-dimensional statement and their verification.

The gaseous phase consists of $N+1$ immiscible components which are the combustion products of powder elements (enumeration is from 1 to N) and the only neutral gaseous phase component – air (subscript $N+1$). The gaseous phase component with the subscript j is characterized with the porosity-averaged density ρ_j:

$$\rho_j = \varphi_j \rho_{0j} / \varphi,\ \rho = \sum_{j=1}^{N+1} \rho_j,\ \varphi = \sum_{j=1}^{N+1} \varphi_j,$$

where φ_j and ρ_{0j} – volume fraction and true density of the j-th gaseous phase component, ρ – total average gaseous phase density, φ – porosity. Dispersed phase in turn consists of N components corresponded to the different powder types and characterized by the volume fractions β_j, moreover

$$\beta = 1 - \varphi = \sum_{j=1}^{N} \beta_j.$$

The system of equations for the modeling of two-dimensional (2D) axisymmetrical gas-powder mixture flow expresses in differential form the fundamental laws of mass, impetus and energy conservation for gaseous and dispersed phases. Equations for the gaseous phase are:

$$\begin{cases} \dfrac{\partial(\varphi\rho_j)}{\partial t} + \dfrac{\partial(\varphi\rho_j u_1)}{\partial r} + \dfrac{\partial(\varphi\rho_j u_2)}{\partial z} = m_j - \dfrac{u_1}{r}\varphi\rho_j,\ j = 1,\ldots,N, \\ \dfrac{\partial(\varphi\rho_{N+1})}{\partial t} + \dfrac{\partial(\varphi\rho_{N+1} u_1)}{\partial r} + \dfrac{\partial(\varphi\rho_{N+1} u_2)}{\partial z} = -\dfrac{u_1}{r}\varphi\rho_{N+1}, \\ \dfrac{\partial(\varphi\rho u_1)}{\partial t} + \dfrac{\partial\left(\varphi\left[\rho u_1^2 + p\right]\right)}{\partial r} + \dfrac{\partial(\varphi\rho u_1 u_2)}{\partial z} = p\dfrac{\partial\varphi}{\partial r} + \sum_{j=1}^{N}\left(\boldsymbol{\Pi}_j\right)_r - \dfrac{u_1}{r}\varphi\rho u_1, \\ \dfrac{\partial(\varphi\rho u_2)}{\partial t} + \dfrac{\partial(\varphi\rho u_1 u_2)}{\partial r} + \dfrac{\partial\left(\varphi\left[\rho u_2^2 + p\right]\right)}{\partial z} = p\dfrac{\partial\varphi}{\partial z} + \sum_{j=1}^{N}\left(\boldsymbol{\Pi}_j\right)_z - \dfrac{u_1}{r}\varphi\rho u_2, \\ \dfrac{\partial(\varphi\rho E)}{\partial t} + \dfrac{\partial(\varphi\rho J u_1)}{\partial r} + \dfrac{\partial(\varphi\rho J u_2)}{\partial z} = -\dfrac{\partial(\beta p v_1)}{\partial r} - \dfrac{\partial(\beta p v_2)}{\partial z} + \sum_{j=1}^{N} Q_j - \dfrac{u_1}{r}\varphi\rho J, \end{cases} \quad (1)$$

Here (r, z) – radial and axial coordinates, u_1 and u_2 – radial and axial components of gaseous phase velocity $\mathbf{u}$, p – gaseous phase pressure, E and e – specific total and internal energy of the gas, v_1 and v_2 – radial and axial components of dispersed phase velocity $\mathbf{v}$, $J = E + p / \rho$ – specific total gaseous phase enthalpy, m_j, $\boldsymbol{\Pi}_j$ and Q_j, j = 1, ..., N,

correspondingly, the rates of mass, impetus and energy change of gaseous phase per unit of volume due to the combustion of powder elements and inter-phase interaction. The correlation between thermodynamics state parameters for gaseous phase is described by the Dupre-type equations with the effective values of specific ratio, covolume and molecular weight [8].

Equations of mass and impetus conservation for the dispersed phase are the following:

$$\begin{cases} \dfrac{\partial(\beta_j\delta_j)}{\partial t}+\dfrac{\partial(\beta_j\delta_j v_1)}{\partial r}+\dfrac{\partial(\beta_j\delta_j v_2)}{\partial z}=-m_j-\dfrac{v_1}{r}\beta_j\delta_j,\ j=1,\ldots,N, \\ \dfrac{\partial(\beta\delta v_1)}{\partial t}+\dfrac{\partial(\beta\delta v_1^2+\beta\sigma)}{\partial r}+\dfrac{\partial(\beta\delta v_1 v_2)}{\partial z}=-\beta\dfrac{\partial p}{\partial r}-\sum\limits_{j=1}^{N}(\mathbf{\Pi}_j)_r-\dfrac{v_1}{r}\beta\delta v_1, \\ \dfrac{\partial(\beta\delta v_2)}{\partial t}+\dfrac{\partial(\beta\delta v_1 v_2)}{\partial r}+\dfrac{\partial(\beta\delta v_2^2+\beta\sigma)}{\partial z}=-\beta\dfrac{\partial p}{\partial z}-\sum\limits_{j=1}^{N}(\mathbf{\Pi}_j)_z-\dfrac{v_1}{r}\beta\delta v_2, \end{cases} \quad (2)$$

where δ_j – bulk density of the j-th component of dispersed phase, δ – average bulk density of dispersed phase, σ – intergranular pressure which is introduced to prevent the unreasonable dispersed phase compaction.

Particular expressions for the terms m_j, $\mathbf{\Pi}_j$ and Q_j which describe inter-phase interaction as well the expression for the dependency of intergranular pressure from the total volume fraction of the dispersed phase β are presented in [7].

It is also convenient to consider the set of equations (1) – (2) in vector form by introducing the vector of conservative variables and the flux vectors:

$$\frac{\partial\mathbf{q}}{\partial t}+\frac{\partial\mathbf{f}}{\partial r}+\frac{\partial\mathbf{g}}{\partial z}=\mathbf{S}_p+\mathbf{S}_m+\mathbf{S}_r, \quad (3)$$

where $\mathbf{q}$ – vector of conservative variables, $\mathbf{f}$ and $\mathbf{g}$ – flux vectors, $\mathbf{S}_p$, $\mathbf{S}_m$ and $\mathbf{S}_r$ – right-hand side vectors, corresponded to the pressure term, inter-phase interaction and source term due to the axial symmetry.

3 Numerical algorithm and parallelization

The calculation of gas-powder mixture motion is based on the integral representation of the determinative system of equations (3) and finite volume approach. If Ω is some 2D closed domain in (r, z) plane with the boundary Γ equations (3) are depressed to the following integral relationships:

$$\frac{\partial}{\partial t}\left[\int_\Omega \mathbf{q}\,d\Omega\right]+\int_\Gamma(\mathbf{f}n_r+\mathbf{g}n_z)\,ds=\int_\Omega\mathbf{S}_p\,d\Omega+\int_\Omega\mathbf{S}_m\,d\Omega+\int_\Omega\mathbf{S}_r\,d\Omega, \quad (4)$$

where $\mathbf{n} = (n_r, n_z)$ – local external normal vector to the boundary Γ. The application of this integral relationship successively to each computational cell Ω_i gives the system of discrete algebraic equations to obtain the cell-averaged conservative flux for the next time step $n+1$:

$$\mathbf{q}_i^{n+1}=\mathbf{q}_i^n-\frac{1}{\omega_i}\int_{t^n}^{t^{n+1}}\left[\sum_i(\mathbf{f}n_r+\mathbf{g}n_z)_i\,s_i\right]dt+\int_{t^n}^{t^{n+1}}\left[(\mathbf{S}_p)_i+(\mathbf{S}_m)_i+(\mathbf{S}_r)_i\right]dt, \quad (5)$$

where ω_i – the area of control volume Ω_i, s_i – the edge length, the right-hand side summation is performed over all the cell edges.

The following discretization of (5) is based on the physical processes splitting procedure [9]. Gas dynamics (subscript g) is described by the following system of equations:

$$\mathbf{q}_{gi}^{n+1}=\mathbf{q}_{gi}^n-\frac{1}{\omega_i}\int_{t^n}^{t^{n+1}}\left[\sum_i(\mathbf{f}_g n_r+\mathbf{g}_g n_z)_i\,s_i\right]dt+\int_{t^n}^{t^{n+1}}\left[(\mathbf{S}_{pg})_i+(\mathbf{S}_{rg})_i\right]dt, \quad (6)$$

dispersed phase (subscript s) – by the equations:

$$\mathbf{q}_{si}^{n+1}=\mathbf{q}_{si}^n-\frac{1}{\omega_i}\int_{t^n}^{t^{n+1}}\left[\sum_i(\mathbf{f}_s n_r+\mathbf{g}_s n_z)_i\,s_i\right]dt+\int_{t^n}^{t^{n+1}}\left[(\mathbf{S}_{ps})_i+(\mathbf{S}_{rs})_i\right]dt. \quad (7)$$

The phases state changing due to the processes of inter-phase interactions as a result of powder elements combustion, relaxation processes and powder elements heating are expressed by the equations:

$$\mathbf{q}_i^{n+1}=\mathbf{q}_i^n+\int_{t^n}^{t^{n+1}}(\mathbf{S}_m)_i\,dt. \quad (8)$$

During the solution of equations (6) the dispersed phase parameters $\mathbf{q}_s$ are considered to be constant, and in equations (7) in contrast the parameters of gaseous phase $\mathbf{q}_g$ are fixed. Discretization of (6) and (7) is performed in a

single manner with the use of interpolation predictor-corrector scheme with the second order of approximation on time and spatial variables. Flux approximation on the cell edges in case of porosity continuity is realized with the use of Godunov's scheme [9]. In other case the linearization of Roe [10] is used. Solution of the equation (8) of the third stage is carried out by the backward differentiation formulas.

The special attention should be paid to the approach which is used for the description of throwing body motion over the non-moving Cartesian grid. The idea of the method is borrowed from the immersed boundary method [11], [12] that was originally developed for the problems of incompressible fluid.

The main advantages of the method are the following:

(a) the method doesn't demand computational grid regeneration,

(b) computational grid is generated in the domains with relatively simple shapes,

(c) reinterpolation of grid data is not necessary,

(d) the possibility of high-quality grid generation and high-accuracy numerical scheme realization.

The calculation by immersed boundary method is performed in a single manner in the whole domain including the areas occupied with solid objects. So the method is good for parallel computations.

Consider again some 2D domain Ω bounded by the smooth curve Γ. Let $\mathbf{n}$ – external normal to the Γ. Let S is a solid body boundary which interacts with the gas. The influence of the solid body to the flow can be taken into account by introduction to the right-hand side of the equations the effective flux vector $\mathbf{F}_w$. The system (4) is then modified in the following manner:

$$\frac{\partial}{\partial t}\left[\int_{\Omega}\mathbf{q}d\Omega\right]+\int_{S}\left(\mathbf{f}n_r+\mathbf{g}n_z\right)ds=\int_{\Omega}\mathbf{S}_p d\Omega+\int_{\Omega}\mathbf{S}_m d\Omega+\int_{\Omega}\mathbf{S}_r d\Omega-\int_{\gamma(\Omega)}\mathbf{F}_w d\Gamma, \tag{9}$$

where $\gamma(\Omega)=\Omega\cap S$. The flux $\mathbf{F}_w$ should prevent mass, impetus and energy losses at the boundary $\gamma(\Omega)$ due to the gas leakage and generate pressure impetus equivalent to the impetus from the gas – body surface interaction:

$$\mathbf{F}_{gw}=\begin{bmatrix}\varphi\rho_j\left(\mathbf{u}-\mathbf{U}_s,\mathbf{n}\right)\\ \varphi\rho\left(\mathbf{u}-\mathbf{U}_s,\mathbf{n}\right)\mathbf{u}+\varphi\left(p-p_w\right)\mathbf{n}\\ \varphi\rho\left(\mathbf{u}-\mathbf{U}_s,\mathbf{n}\right)E+\varphi\left(p\mathbf{u}-p_w\mathbf{U}_s,\mathbf{n}\right)\end{bmatrix},\ \mathbf{F}_{sw}=\begin{bmatrix}\delta_j\beta_j\left(\mathbf{v}-\mathbf{U}_s,\mathbf{n}\right)\\ \delta\beta\left(\mathbf{v}-\mathbf{U}_s,\mathbf{n}\right)\mathbf{v}+\beta\left(\sigma-\sigma_w\right)\mathbf{n}\end{bmatrix}. \tag{10}$$

Here p_w – pressure on the surface S from the gas – body surface interaction, σ_w – intergranular pressure on the surface S from the dispersed phase – body surface interaction, $\mathbf{U}_s$ – local velocity vector of body surface. If Ω is a domain so that $\gamma(\Omega)=\varnothing$ then the system of equations (9) evidently equivalent to the standard system of equations for multicomponent multiphase medium motion. If one choose Ω so that $\gamma(\Omega)\neq\varnothing$ and the volume of Ω goes to zero equations (9) – (10) are reduced to the relationships $\mathbf{u}=\mathbf{v}=\mathbf{U}_s$, $p=\sigma=p_w$, which are the boundary conditions for the set of equations for gas dynamics for a solid wall.

The numerical scheme in case of existence of a solid objects in a flow is constructed then in a follow manner. At the first stage the pass-through calculation by the schemes (6) – (8) is carried out. At that the existence of the solid body surface is not taken into account. Obtained solution vector $\tilde{\mathbf{q}}_i^{n+1}$ is the modified as:

$$\mathbf{q}_i^{n+1}=\tilde{\mathbf{q}}_i^{n+1}-\frac{\Delta t}{\omega_i}\sum_{\gamma}\left(\mathbf{F}_w\right)_{\gamma}^{n+1}s_{\gamma}, \tag{11}$$

where s_γ is the length of the curve $S_\gamma\cap\Omega_i$ and the summation is performed over the constituent elements S_γ of contour S. The iterative procedure is used to solve (11). The numerical solution obtained has a sense only for the computational cells which are outer for the object of are intersected by it.

Numerical algorithm parallelization is based on the domain decomposition method. Computational domain is subdivided into the cells that are converted to the graph in which each node corresponds to the cell and each edge means the geometric neighborhood between some cells. The graph is decomposed on approximately equivalent parts with the use of the open source METIS package (see Fig. 2).

Each computational unit processes its own subdomain, the exchange of data from the boundary cells occurs at the end of each time step. The exchange is organized in the following manner. The computational units connection graph is built. The nodes of the graph are the units, two nodes are connected with the edge if there is at least one computational cell on one unit that has a neighbor on the other.

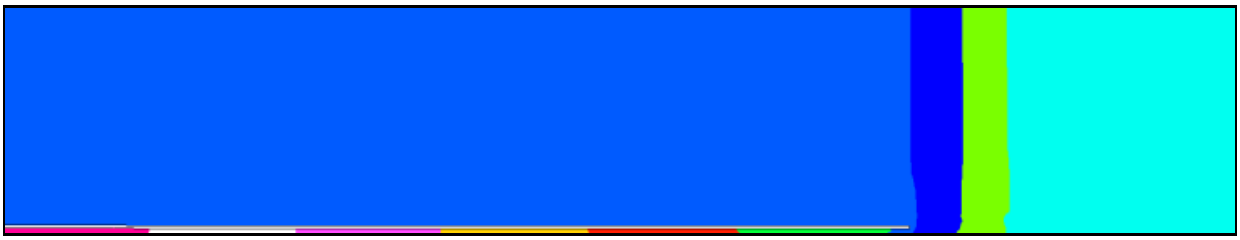

Fig. 2. Example of METIS decomposition into 10 parts of the typical computational domain for 2D axisymmetrical internal and intermediate ballistics calculation

All the numerical experiments are performed with the use of computational resources of Joint Supercomputer Center Russian Academy of Sciences and Moscow State University Supercomputer Complex.

4 Statement of the problem

The weapon used in the numerical investigations is a 20 mm cannon with a shot travel of 1.43 m and a chamber volume of $4.17 \cdot 10^{-5}$ m^3 [13] so the chamber length is considered to be 0.13 m. The projectile is that of the standard M55A2 training round (inert) weighting 0.098 kg with elongation 3.75. The forcing pressure is taken equal to 150 atm. The propellant for this round is WC870 ball powder with the properties presented in Tab. 1.

Tab. 1. Properties of WC870 ball powder

Property	***Value***	***Source***
Force	0.98 MJ/kg	[13]
Covolume	982 cm^3/kg	[3]
Specific heat ratio	1.24	[13]
The burning arch thickness	0.775 mm	[14]
Form coefficients	$\chi = 3.0$, $\lambda = -1.0$, $\mu = 1/3$	Standard for ball powders, [8]
Burning temperature	2577 K	[5]
Burning law	$(0.256 \cdot 10^{-5}) \cdot p^{0.7}$ m/ms, p in MPa	[15]

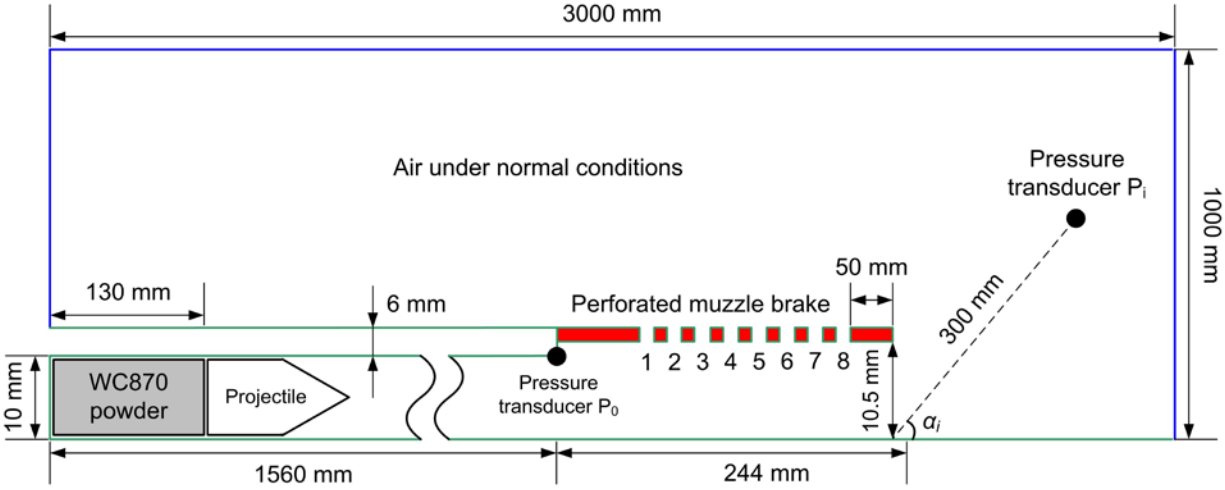

Fig. 3. Schematic statement of the problem

The same cannon was also used in [3], [5], [6] and [13] for numerical and experimental investigations of blast levels for the both bare muzzle shot and perforated MB. The statement of the problem is schematically depicted in Fig. 3. The blue boundaries correspond to the outlet boundary condition, the green ones – to the impermeability condition. The powder is uniformly distributed in chamber, the charge ignition period is not taken into account because there is no information about initiation system in [3], [5], [6], [13].

First of all it was necessary to perform internal ballistics processes calculations in quasi-one-dimensional statement to check the adequacy of the constructed model. Five numerical experiments with the use of BARS-1MP program [16] for the different charge masses were carried out: 38.9 g, 25.9 g, 17.8 g, 9.7 g and 3.6 g (see Section 5). Then the analogous numerical experiments were repeated but in the 2D axisymmetrical statement (see Fig. 3 without red parts corresponded to the MB). The goal for that was to investigate the parameters of the shock wave which forms before the

moving projectile in the barrel (see Section 6). The exhaust properties of the propellant gases were measured using pressure transducer P0 located at the muzzle.

The last two numerical experiments were the shots with the barrel elongation – with (see Fig. 3, digits from 1 to 8 correspond to the number of the vent) and without perforation (see Section 6). The geometry of perforated MB was taken from [6] and was corresponded to the scaled brake for the 120 mm cannon. The brake has eight rows of circular vents. Each row has twelve vents uniformly spaced around the tube circumference. The four rows nearest to the breech have smaller diameter vents based on stress considerations.

The holes diameters for 2D axisymmetrical statement were defined by the condition of venting area preserving: $D_1 = D_2 = D_3 = D_4 = 2$ mm, $D_5 = D_6 = D_7 = D_8 = 2.5$ mm. The distances between the holes are the following: $r_{12} = r_{23} = r_{34} = r_{45} = 6$ mm, $r_{56} = 5.5$ mm, $r_{67} = 5$ mm, $r_{78} = 4.5$ mm. Seven pressure transducers were used, placed at angles $\alpha_1 = 15°$ (transducer P1 and so on), $\alpha_2 = 30°$, $\alpha_3 = 60°$, $\alpha_4 = 90°$, $\alpha_5 = 120°$, $\alpha_6 = 150°$ and $\alpha_7 = 165°$ with respect to the line of fire and at radius of 30 calibers from the muzzle. In all 2D calculations the minimal cell size is 0.5 mm, the best grid resolution is near the muzzle.

5 Internal ballistics simulations in 1D statement

In natural experiments [5] the muzzle velocity and projectile bottom pressure at the moment when projectile moved out from the barrel were fixed. The typical distribution of the mentioned parameters are presented in Fig. 4.

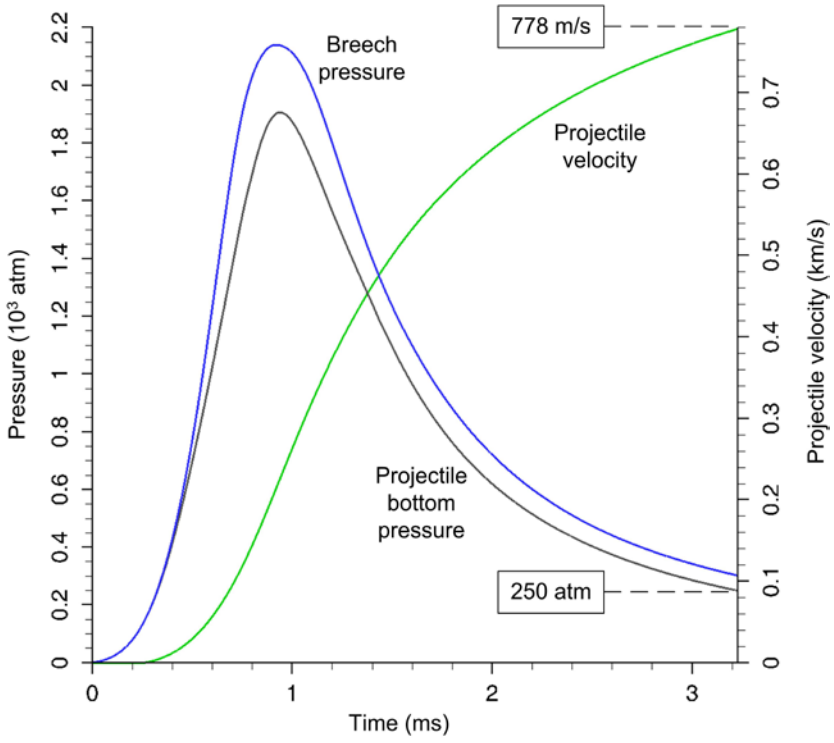

Fig. 4. Internal ballistics process in quasi-one-dimensional statement for the charge mass 25.9 g

Tab. 2 demonstrates the comparison of calculated and experimental projectile muzzle velocity for the different charge masses. As one can see the dynamics of this value change in numerical experiments is correct that means the correctness of internal ballistics processes description and the possibility of further 2D investigations.

Tab. 2. Results of numerical experiments in quasi-one-dimensional statement

Charge mass, g	*Calculated muzzle velocity, m/s*	*Experimental muzzle velocity, m/s*
38.9	1032	1050
25.9	778	775
17.8	615	615
9.7	431	463
3.6	260	280

6 Internal and intermediate ballistics simulations in 2D statement

A number of 2D axisymmetrical calculations was made to investigate the gun tube empting and muzzle blast flow features. As is it known [5] the flow from the muzzle of a gun can be subdivided on two stages. The first, or precursor flow, develops as the air in the gun tube is forced out ahead of the accelerating projectile (see Fig. 5a). The second, or propellant gas flow, develops when these high pressure gases are released following projectile separation (see Fig. 5b).

The muzzle pressures associated with these two flows are vastly different. For example, in the numerical experiment at the launch velocity 1050 m/s corresponded to the charge mass 38.9 g the precursor muzzle pressure obtained at P0 transducer is approximately 12.4 atm (the experimental value – 16.3 atm [5]) and a propellant gas muzzle pressure is about 365 atm (the experimental value – 287 atm [5]).

The order of magnitude change in pressure at the muzzle following shot ejection results in rapid expansion of the propellant gases over the projectile and through the boundaries of the precursor jet. However, the presence of the precursor flow does effect the development of the propellant gas blast. Since the propellant gas expands into a heated, moving precursor flow, the initial conditions for the formation of blast are not those of an expansion into a static ambient. Note also that calculated precursor wave velocity 1.1 km/s is close to the experimental value 1.3 km/s [5].

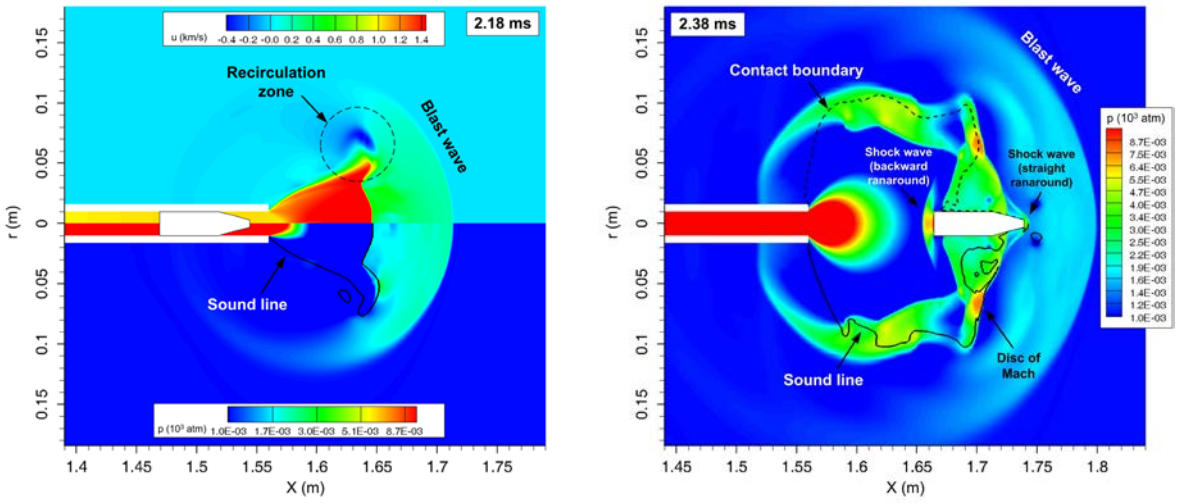

(a) (b)

Fig. 5. Flow structure for bare muzzle shot at different time moments, charge mass 38.9 g, *u* is the axial component of gaseous phase velocity

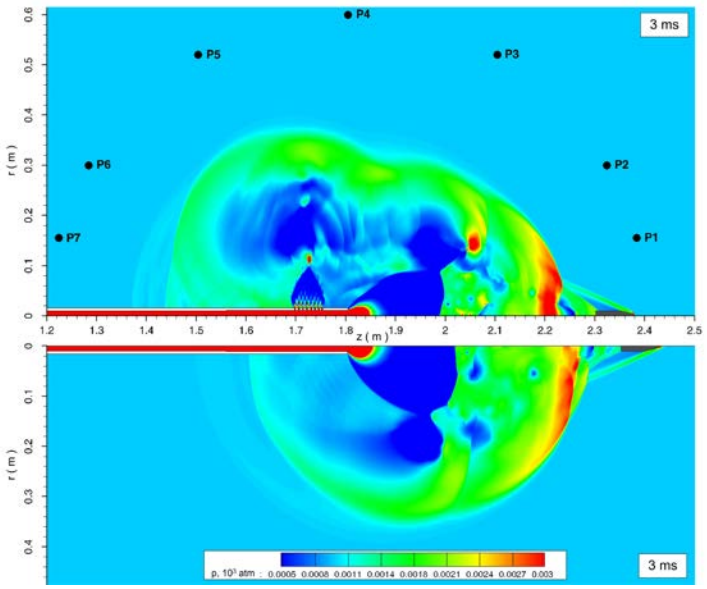

Fig. 6. Pressure fields for the shots with MB (upper half) and with bare barrel extension (lower one)

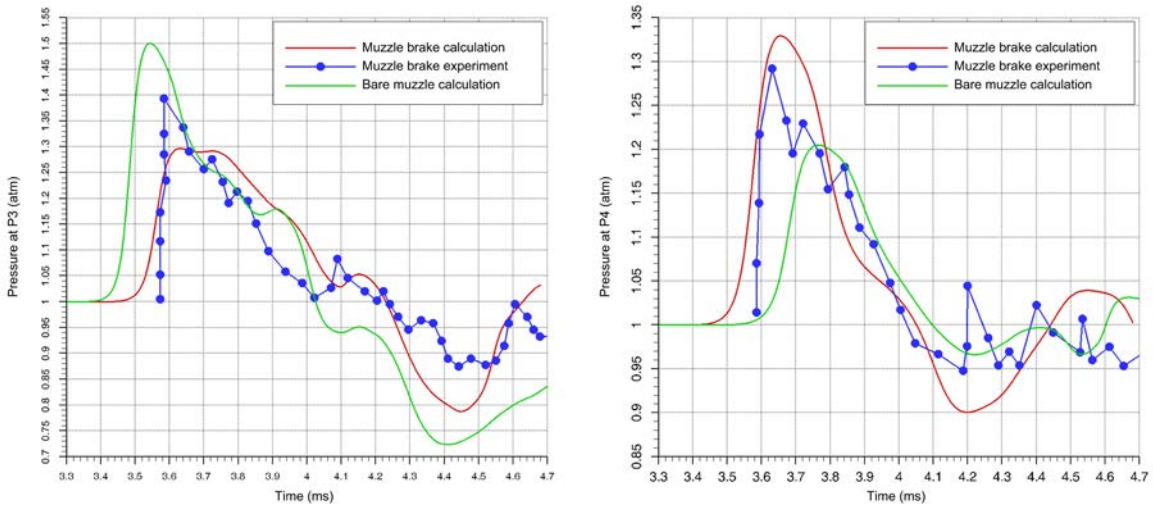

Fig. 7. Comparison of pressures at transducers P3 (left) and P4 (right) in MB calculation (red line), MB experiment [6] (blue line with points) and bare barrel extension calculation (green line)

The principle effect of venting is seen to be the generation of a more uniform blast field around the cannon [3], [6] (see Fig. 6). The disturbance is diminished somewhat downstream of the muzzle and considerably strengthened upstream (see Fig. 7).

For pressure transducers P1, P2 and P3 the peak overpressure for bare muzzle shot is higher than for the perforated MB shot. Beginning from the pressure transducer P4 and further – P5, P6 and P7 – perforated brake blast level is significantly higher. At the same time the calculated perforated muzzle brake blast levels are in good agreement with experimental data (see Fig. 7).

7 Conclusion

The simultaneous solution of the internal and intermediate ballistics problems is carried out for the cannon with bare muzzle and perforated muzzle brake shots. The mathematical model of multiphase multicomponent two-velocity gas-powder continuum motion with inter-phase interaction and the corresponding numerical algorithm used the immersed boundary method are described in detail. The main features of parallelization techniques are also discussed.

A series of preliminary internal ballistics calculations in quasi-one-dimensional statement and the bare muzzle flow and blast wave numerical investigations in two-dimensional axisymmetrical case are performed. Results of internal ballistics calculations and the precursor muzzle wave parameters are verified with the use of experimental data [5].

Near-muzzle blast levels for perforated muzzle brake at the distance of 30 calibers for different angles are in good agreement with experimental data [6].

8 Acknowledgements

The work is supported by the Russian Foundation for Basic Research (grant No. 11-01-12120-ofi-m-2011) and by the scholarship of President of the Russian Federation for young scientists and Ph.D. students which perform promising scientific investigations and developments in top-priority modernization fields of Russian economy on 2012 – 2014. The authors express their deep appreciation to Dr. V.V. Chernov (JSC «CRI «Burevestnik») for contribution for this investigation.

References

[1] I. I. Jukov et al.: Artillery equipment. Moscow: Mashinostroenie, 1975.
[2] B. V. Orlov et al.: Arrangement and designing of the artillery weapon barrels. Moscow: Mashinostroenie, 1976.
[3] G. C. Carofano: A comparison of experimental and numerical blast data for perforated muzzle brakes. *US army armament research, development and engineering center, Technical report ARCCB-TR-90034*, 1990.
[4] V. V. Sadovsky, M. V. Jarkov, P. I. Karasev, A. A. Aksenov: Solution of the problem about the multichamber muzzle brake effectiveness definition. *URL: http://www.tesis.com.ru/software/flowvision/fv_exp.php*, 2012.
[5] E. M. Schmidt, E. J. Gion, K. S. Fansler: A parametric study of the muzzle blast from a 20 mm cannon. *US army armament research and development command, Ballistic res. lab., Technical report ARBRL-TR-02355*, 1981.

[6] G. C. Carofano: Perforated brake efficiency measurements using a 20-mm cannon. *US army armament research, development and engineering center, Technical report ARCCB-TR-93010*, 1993.
[7] I. V. Semenov, P. S. Utkin, I. F. Akhmedyanov, I. S. Menshov: Application of high performance computing to the solution of interior ballistics problems. *Numerical Methods and Programming*, 12:183-193, 2011.
[8] Yu. P. Khomenko, A. N. Ischenko, V. Z. Kasimov: Mathematical Modelling of Interior Ballistic Processes in Barrel Systems. Novosibirsk: Publishing House of SB RAS, 1999.
[9] E. F. Toro: Riemann Solvers and Numerical Methods for Fluid Dynamics. Springer, 2nd ed., 1999.
[10] D. Rochette, S. Clain, T. Buffard: Numerical scheme to complete a compressible gas flow in variable porosity media. *International Journal of Computational Fluid Mechanics*, 19(4): 299-309, 2005.
[11] R. Mittal, G. Iaccarino: Immersed Boundary Methods. *Annu. Rev. Fluid Mech.*, 37: 239-261, 2005.
[12] D. Kim, H. Choi: Immersed boundary method for flow around an arbitrarily moving body. *Journal of Computational Physics*, 212: 662-680, 2006.
[13] R. E. Jr. Dillon, H. T. Nagamatsu: An experimental study of perforated muzzle brakes. *US army armament research and development center, Technical report ARLCB-TR-84004*, 1984.
[14] D. E. Kooker, L. M. Chang, S. L. Howard: Flamespreading in Granular Solid Propellant: Design of an Experiment. *US Army Research Laboratory Report ARL-MR-80*, 1993.
[15] D. Mickovic: Treatment of Deterred Propellants in Interior Ballistic Calculations. *FME Transactions*, 38(3):137-141, 2010.
[16] I. V. Semenov, I. S. Menshov, I. F. Akhmedyanov, P. S. Utkin, V. V. Markov: State Registration Certificate No. 2011610905 for computer program “BARS-1MP”, 2011.